RSC Advances

PAPER

View Article Online
View Journal | View Issue

Cite this: *RSC Adv.*, 2023, **13**, 7963

Molecular dynamics study on the thermodynamic stability and structural evolution of crown-jewel structured PdCu nanoalloys

Qing Liu, Yajing Zhang and Ping Qian *

The novel crown-jewel (CJ) structured PdCu nanoalloys have attracted considerable interest in high-performance single-atom catalysis. The characteristics of demanding high-temperature calcination in the synthesis of these samples disable us from experimentally understanding the details of the thermal evolution behavior of PdCu nanoclusters during the heating process. In this work, by analyses of potential energy surface, bond order parameter, and radial distribution function, we have theoretically studied the thermodynamic stabilities and structural evolution of Pd-decorated Cu-based CJ nanoclusters with various compositions and sizes by molecular dynamics simulations. PdCu nanoclusters undergo a cuboctahedral (Cubo) to icosahedral (Ico) structural transformation before melting. This transformation is size- and Pd-composition dependent. The small size and high Pd-composition of PdCu nanoclusters facilitate this transformation. In addition, we find that the surface and interface effects of clusters have an important impact on the structural transformation and Cubo–Ico structural transformation is strongly related to the release of excess energy.

Received 16th December 2022
Accepted 23rd February 2023

DOI: 10.1039/d2ra08024a

rsc.li/rsc-advances

1. Introduction

Bimetallic nanoclusters (NCs) have gained increasing attention in catalysis for their significant catalytic performance due to the size effect and large surface-volume ratio.[1,2] They have distinctive properties from the corresponding unary nanoclusters because of the synergistic effects between different elements.[3] By designing different kinds of structural models, such as the mixed alloy,[4] quasi-Janus,[5] core@shell,[6,7] onion-like A–B–A,[8] and crown-jewel (CJ) structures,[9] the unique properties can be achieved for bimetallic nanoclusters, making them suitable for widespread applications in catalysis. Especially the NCs with CJ structure, where one metal cluster serves as the crown and other metal atoms serve as the jewels decorating the special positions of the crown, is considered a novel single-atom catalyst.[10,11] For example, recent reports have presented that PdAu,[9] IrPdAu,[12] PtFe,[13] and PtAu[14] nanoalloys with CJ structures show significant catalytic activity and selectivity, which is due to the unique electronic structures and coordinative unsaturation of active sites. In a word, crown jewel-structured NCs are worth studying deeply as potential candidates in the field of catalysis.

Pd-based nanoalloy has been considered an attractive alternative to Pt catalysts as Pd has similar catalytic properties as Pt. Alloying Pd with cheap metals will significantly reduce the high cost of precious metal catalysts and also enhance the catalytic activity.[15–18] The improved catalytic performance is attributed to the modification of the electronic structures of Pd upon bonding with the alloying metals.[19] Among these alloy catalysts, PdCu nanoalloys have been extensively studied as electrocatalysts, which show excellent catalytic performance for oxygen reduction reaction (ORR) and hydrogen evolution reaction (HER) because of the strong synergistic effect. For instance, Kariuki *et al.* prepared the monodisperse Pd–Cu nanoparticles by a colloidal synthesis methodology.[20] The results show that carbon-supported Pd–Cu catalysts have excellent catalytic properties for ORR in an acidic condition. Tang *et al.* studied the effect of alloy compositions on ORR activity trends for PdCu nanoparticles.[4] The results show that the average oxygen binding reduces as Cu is added to Pd, indicating an increase in catalytic activity up to a peak at the 1 : 1 Pd/Cu ratio. In addition, Zhang *et al.* synthesized CuPd nanocrystals with different non-spherical shapes by adjusting the concentrations of reactants.[21] The results reveal that the ORR activity of CuPd is remarkably shape-dependent. Elham Chiani *et al.* synthesized PdCu nanoparticles decorated on mesoporous silica and carbon nanotubes.[22] They proposed a potential strategy to develop stable and highly efficient HER catalysts. In addition, Michelle *et al.* synthesized ultrathin PdCu alloy nanowires.[23] They found that the PdCu nanostructure containing an intermetallic B_2 phase exhibits improved HER electrocatalytic performance in alkaline and acid environments.

As the nanoalloy with the crown-jewel structure is emerging as an important focus in catalytic applications, it is reported

Beijing Advanced Innovation Center for Materials Genome Engineering, Beijing Key Laboratory for Magneto-Photoelectrical Composite and Interface Science, School of Mathematics and Physics, University of Science and Technology Beijing, Beijing, 100083, China. E-mail: qianping@ustb.edu.cn

that PdCu nanoalloys with the crown-jewel structure are promising candidates for high-performance and cost-effective single-atom catalysts.[24] However, theoretical investigation on the structural properties and thermodynamic stabilities of the CJ-structured PdCu nanoclusters has rarely been reported, which is important for the practical application of PdCu catalysts. This study is also motivated by the fact that the synthesis of nanoclusters usually requires high calcination temperatures. Therefore, understanding how the heating process affects the structural stabilities and atomic arrangements of alloy nanoclusters is crucial for designing high-performance catalysts. If the nanocluster is vulnerable to operating conditions, the occurrence of interatomic diffusion or atomic rearrangement may render the reaction futile.[25]

In this work, we studied the heating process of PdCu nanoalloys with various types of crown-jewel structures by molecular dynamics (MD) simulation and explored the effects of cluster size and composition on the structural evolution and thermodynamic stability of PdCu nanoclusters. Interestingly, we found a structural transition from the cuboctahedral (Cubo) structure to the icosahedral (Ico) structure in some PdCu nanoclusters during heating. The structural transition may alter the nanocluster's catalytic capacity. As discussed in our previous paper,[24] the configuration (cuboctahedral and icosahedral) of the PdCu cluster has an important impact on the HER and ORR catalytic activity. Different configurations will have different catalytic properties. In addition, we also explored the conditions and the influencing factors of the structural transformation from the Cubo structure to the Ico structure (Cubo–Ico).

2. Models and computational methods

We investigated the structural evolution and thermodynamic stabilities of PdCu alloy clusters by MD simulations. The cuboctahedral configuration is chosen as the initial morphology of the PdCu nanocluster because of being experimentally and theoretically reported as one of the stable structures of free clusters.[26,27] We modeled three types of Pd-decorated crown-jewel Cu-hosted clusters, as shown in Fig. 1, in which Cu atom(s) at a single vertex (referred to as CJ-1 in Fig. 1b), all vertices (CJ-2 in Fig. 1c), and all edges (CJ-3 in Fig. 1d) of cuboctahedral Cu clusters are artificially substituted by Pd. Additionally, the same shaped pure Cu (see Fig. 1a) and Cu@Pd core–shell (Fig. 1e) configurations with all Cu atoms of facets replaced by Pd are also studied for comparison. For each type of structure, size-varied models containing 147, 309, 561, and 923 atoms are used to study the size effects on thermal evolution behavior. The large simulation boxes of $25 \times 25 \times 25$ Å, $30 \times 30 \times 30$ Å, $35 \times 35 \times 35$ Å, and $40 \times 40 \times 40$ Å are adopted for size-varied nanoclusters containing 147, 309, 561, and 923 atoms, respectively, to eliminate the spurious interactions between their artificial periodic images.

We use the embedded atom method[28]-driven MD simulations to investigate the heating process of Pd composition-varied Cu-based nanoalloys, which is implemented in the Large-scale Atomic/Molecular Massively Parallel Simulator (LAMMPS) software.[29] The prediction of MD results is subjected to the accuracy of interatomic interaction potential, and we need to carefully select an appropriate one for PdCu nanoalloy. By introducing the alloy model, Zhou *et al.* have developed a procedure to generalize the EAM potentials with identical analytic forms. This greatly improves the scalability of EAM and makes it suitable for the description of interatomic interactions of alloys with any combination of 16 metals (Cu, Ag, Au, Ni, Pd, Pt, Al, Pb, Fe, Mo, Ta, W, Mg, Co, Ti, and Zr).[30] The accuracy of the EAM form in simulating the structural properties and thermodynamic stabilities of alloy nanoclusters has been verified in previous reports.[24,31–33] We thus select this EAM potential by Zhou *et al.* for all MD simulations of this work. The equations of motion are integrated using the velocity-Verlet algorithm with a time step of 1 fs, and the temperature is controlled by the Nover–Hoover thermostat in heating. The canonical ensemble (NVT) is used in this work. The initial metal clusters are relaxed adequately at 0 K and then heated up to melting-above 1600 K with the temperature step of 20 K. For each temperature step, the first 200 ps were used for the cluster heating, and the next 200 ps were used for the atomic structure equilibration and the statistical averaging. Thus, each temperature step has a duration of 400 ps, with a heating rate of 100 K ns^{-1}.

3. Results and discussion

3.1 Heating process of PdCu nanoclusters

3.1.1 Potential energy surfaces. We calculated the total potential energy surfaces (PESs) during the heating of Cu-based clusters with various Pd surface compositions (Cu, CJ-1, CJ-2, CJ-3, and Cu@Pd) and sizes (N = 147, 309, 561 and 923 atoms). PES is supposed to scale linearly with heating temperature unless some structural transformation or phase transition occurs. As shown in Fig. 2, all nanoclusters with various sizes and Pd compositions have a sudden rise in PES around 900 K, where smaller sizes jump up earlier (see Fig. 2a and b), but larger sizes do later (see Fig. 2c and d), which corresponds to the melting point. The transition temperature from one structure to another can be identified by the sharp jump in the potential energy curve.

Interestingly, there is also a sharp drop in PES before melting. For the smallest size of 147-atom nanoclusters in Fig. 2(a), PESs of pure Cu and CJ-1 configurations have tiny drops at 20 K. By checking the corresponding geometries of configurations, we found that these two nanoclusters both undergo a solid–solid transformation structurally from the cuboctahedral configuration to the icosahedral configuration (Cubo–Ico) at 20 K. The geometry evolution process during heating will be thoroughly discussed in the next sections. The drop in PESs at the transformation temperature indicates that it is exothermic, which is attributed to the total energy difference between the icosahedral (product phase) and cuboctahedral (parent phase) configurations. Besides, we fail to see a similar drop in PES for high Pd-compositions (CJ-2, CJ-3, and Cu@Pd structures) because it happens prematurely at the stage of relaxation of 0 K. Taking CJ-2 configuration of 147-atom PdCu

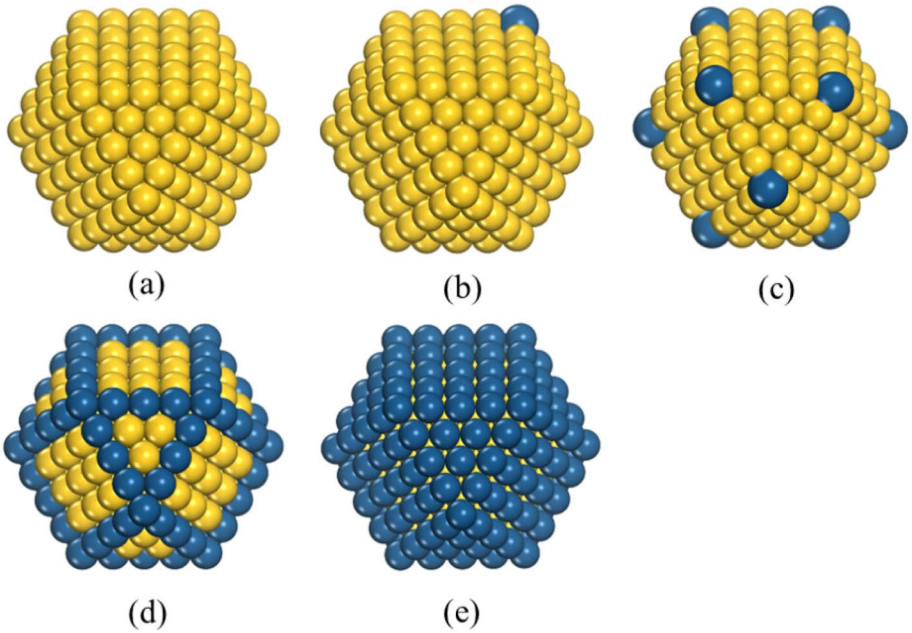

Fig. 1 Schematic structures of cuboctahedral Cu-based nanoclusters with five surface Pd/Cu compositions. (a) Pure Cu, (b) one single vertex-decorated CJ-1 PdCu, (c) all vertices-decorated CJ-2 PdCu, (d) all edges-decorated CJ-3 PdCu, and (e) core–shell Cu@Pd structures. Cu and Pd elements are denoted in yellow and dark blue balls, respectively.

nanocluster as a representative, we demonstrate some structural snapshots taken during the continuous structural transformation for the cuboctahedral cluster at 0 K in Fig. 3. From the figure we found that the Cubo–Ico transition is rapid, diffusion-less, and solid-to-solid structural change occurs through the cooperative displacement of all atoms over very short distances, where atoms maintain a close relationship with one another in the crystal structure.

Similarly, some PdCu nanoclusters with larger sizes (N = 309, 561, and 923 atoms) also undergo the structural transition

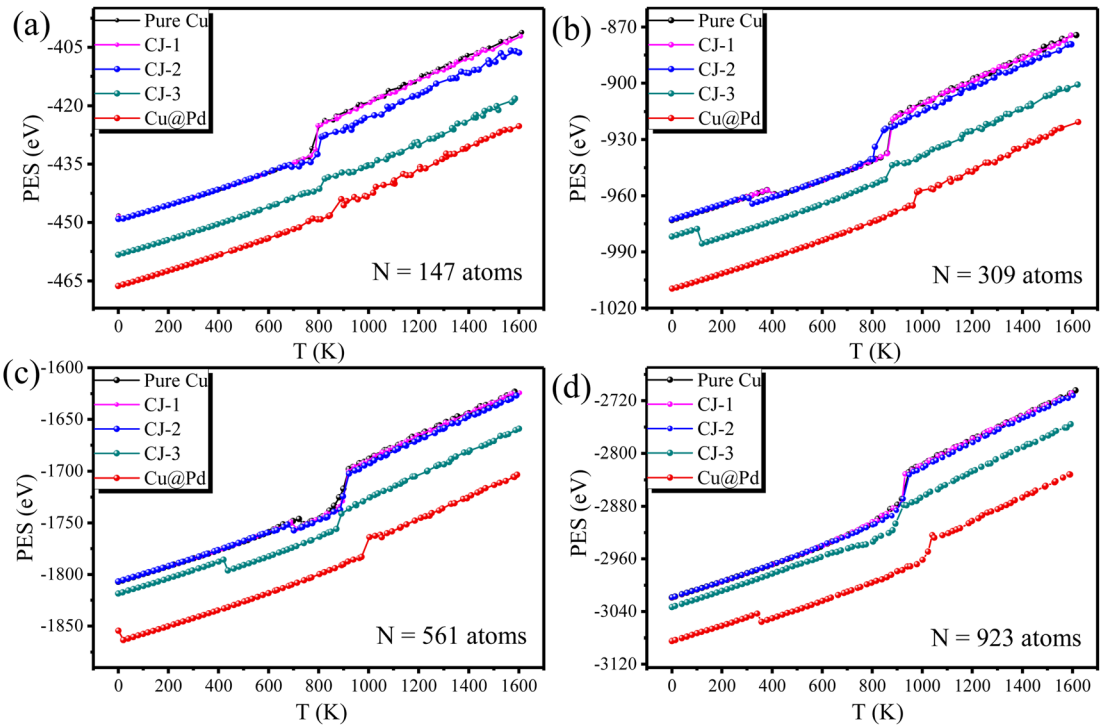

Fig. 2 The PES *versus* the temperature during heating for pure Cu, Pd composition-varied CJ PdCu, and Cu@Pd core–shell nanoclusters. (a) The number of nanoclusters N = 147; (b) N = 309, (c) N = 561, and (d) N = 923.

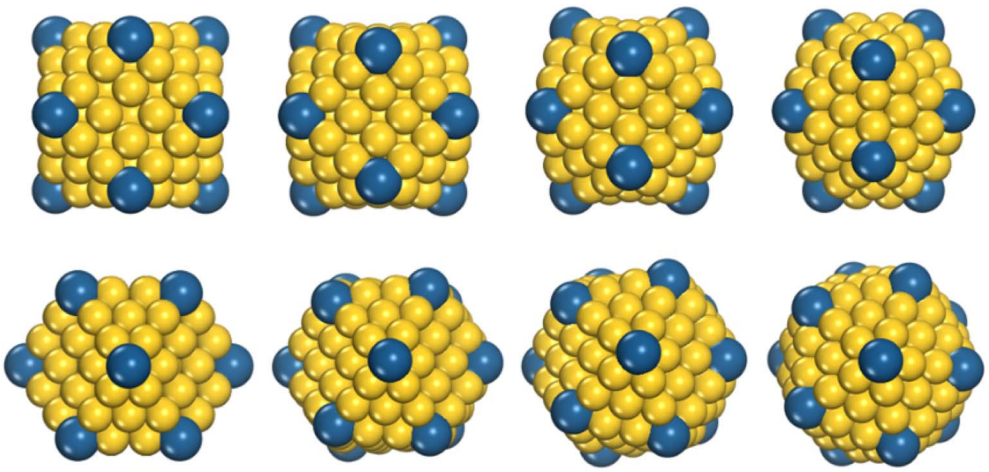

Fig. 3 The top-view and side-view of atomic configuration snapshots showing the structural evolution of 147-atom PdCu nanocluster with CJ-2 during 0 K relaxation.

from Cubo to Ico structure before the melting point. To have a clearer view, we extracted the transition points from Fig. 2 and summarized the solid–solid Cubo–Ico transition temperatures (T_{tran}) and solid–liquid transition temperatures (T_{melt}) *versus* Pd-composition varied nanoclusters with four sizes in Fig. 4.

From Fig. 4, we see the trend that the transformation temperatures decrease with the increasing Pd-composition of nanoclusters for the fixed size, while the 923-atom large size depresses the occurrence of the transformation of pure Cu and CJ structures before solid–liquid transition. It indicates that Cubo–Ico structural transition is strongly related to the cluster size and occurs only in small clusters.

Besides, to investigate the influence of heating rate on the Cubo–Ico transition temperature, we vary the heating rate, and 200 K ns^{-1}, 100 K ns^{-1}, 50 K ns^{-1}, and 25 K ns^{-1} heating rates are used in this work. Taking 309-atom PdCu nanoclusters as an example, we study the heating process of CJ-1, CJ-2, and CJ-3 structures and Cu@Pd nanoclusters, and the Cubo–Ico transition temperatures at different heating rates are shown in Table 1. From the table, we can see that for three kinds of CJ structures, the Cubo–Ico transition temperature has an overall declining trend as the heating rate decreases, but the change is small. For the 309-atom Cu@Pd nanocluster, the transition temperature is always 0 K due to the large interfacial lattice strain. The above indicates that the heating rate has an impact on the Cubo–Ico transition, but the influence is small.

3.1.2 Geometry evolution and radial distribution functions. Apart from PES curves, the structural transformation or phase transition can also be tracked by comparing the differences between structural properties such as the radial

Table 1 The Cubo–Ico transition temperatures at different heating rates for 309-atom PdCu nanoclusters with four surface compositions

Structures	200 K ns^{-1}	100 K ns^{-1}	50 K ns^{-1}	25 K ns^{-1}
CJ-1	422	407	402	381
CJ-2	341	321	303	318
CJ-3	141	120	137	136
Cu@Pd	0	0	0	0

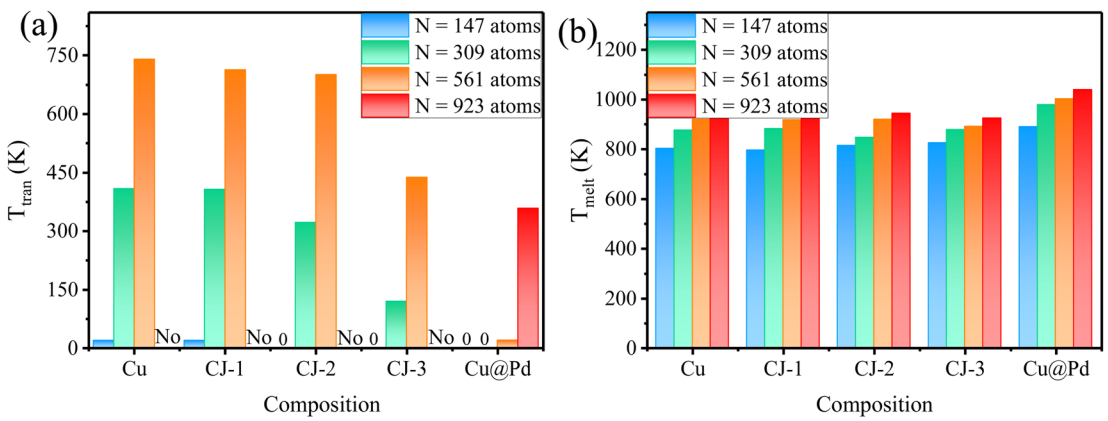

Fig. 4 The distributions of (a) Cubo–Ico transformation temperatures (T_{tran}) and (b) melting temperatures (T_{melt}) of PdCu nanoclusters *versus* compositions with various sizes.

distribution functions (RDFs) and bond order parameter (BOP). RDF is defined as the probability of finding a pair of atoms with a distance of r, relative to the probability expected for a completely random distribution against a homogeneous distribution.[34,35] It can thus be used to analyze the structural changes and the degree of disorder of the nanostructure. Fig. 5 presents the RDFs of 309-atom Cu, CJ-1, CJ-2, CJ-3, and Cu@Pd nanoclusters, accompanied by the corresponding geometric configurations at transition-critical temperatures as insets. RDF gives a series of individual sharp peaks for crystalline phases but broad peaks superimposed on the oscillatory trajectory because of the absence of long-range order characteristics.[36] At 100 K (Fig. 5), all nanoclusters inherit crystalline characteristics from initial states and remain as cuboctahedral (but icosahedral for $Cu_{147}@Pd_{162}$) geometries because of the sharp peaks (also see left images of insets of Fig. 5).

As it heats up to the transformation temperatures, we see the changes in geometry from cuboctahedrons to icosahedrons for Cu cluster and CJ nanostructures in the middle images of insets of Fig. 5, but the crystallinity remains, although a little more broadening of RDF peaks compared to that at 100 K because of the enhanced perturbation of atomic orientation caused by atomic kinetics. When the temperature is further raised to around 900 K, we see the peaks become less and wider, and a clear gap appears between the first two peaks of RDF, which shows the sign of a liquid phase. The highly disordered atom arrangements in the right images of insets of Fig. 5 also supported solid–liquid transition.

In addition, the relative positions between atoms of clusters remain unchanged before and after the Cubo–Ico transformation, indicating the diffusion-less process. Pd atoms always stay at the initial vertex or edge positions, and the crown-jewel structures are well maintained until melting, which further confirms the thermal stabilities of PdCu nanoclusters.

3.1.3 Bond order parameter. The bond order parameter is also an effective way to distinguish solid and liquid states and examine crystalline structures such as face-centered cubic (FCC), body-centered cubic (BCC), hexagonal close-packed (HCP), and ICO types.[37] In this section, we use the bond order parameter $W6$ to differentiate nanoclusters. $W6$ has a set of numerical assignments to quantify crystalline and liquid phases, including −0.013 for FCC, −0.17 for Ico, and 0 for the liquid phase. We present the $W6$ bond order parameters with heating for 309-atom nanoclusters in Fig. 6. At the low-temperature stage ($T < T_{tran}$), all structures (but for $Cu_{147}@Pd_{162}$) maintain initial FCC packing, indicating the Cubo configuration. As temperatures increase and step into the transformation stage ($T_{tran} \leq T < T_{melt}$), $W6$ parameters dump down to near −0.17 from ∼−0.013, indicating a new Ico transformation. $W6$ remains at ∼−0.17 until temperatures go up to melting points and further holds at 0 at the liquid stage ($T \geq T_{melt}$) because of the disorder of liquid structure for all nanoclusters. Our bond order parameter analysis of structural transformation and melting temperatures is in good agreement with that of PESs in Fig. 2(b) and RDFs in Fig. 5.

3.2 Effects of Pd composition on stabilities and transformation temperatures of PdCu nanoclusters

To better understand the role of the Pd component in the structural evolution of PdCu nanoclusters, we plot the

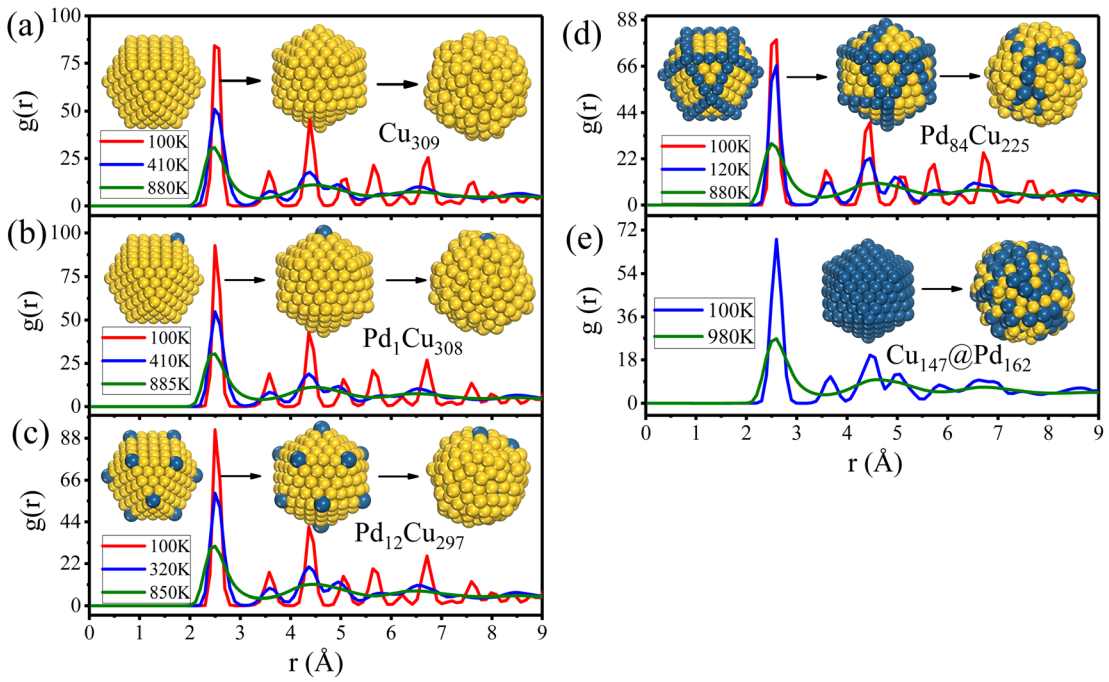

Fig. 5 The calculated RDFs of 309-atom (a) pure Cu_{309}, (b) CJ-1: Pd_1Cu_{308}, (c) CJ-2: $Pd_{12}Cu_{297}$, (d) CJ-3: $Pd_{84}Cu_{225}$, and (e) core–shell $Cu_{147}@Pd_{162}$ nanoclusters. Their corresponding structural snapshots at 100 K, around Cubo–Ico structural transformation (if exists) and melting temperatures during the heating, are displayed as insets, respectively. Cu and Pd atoms are denoted in yellow and dark blue balls.

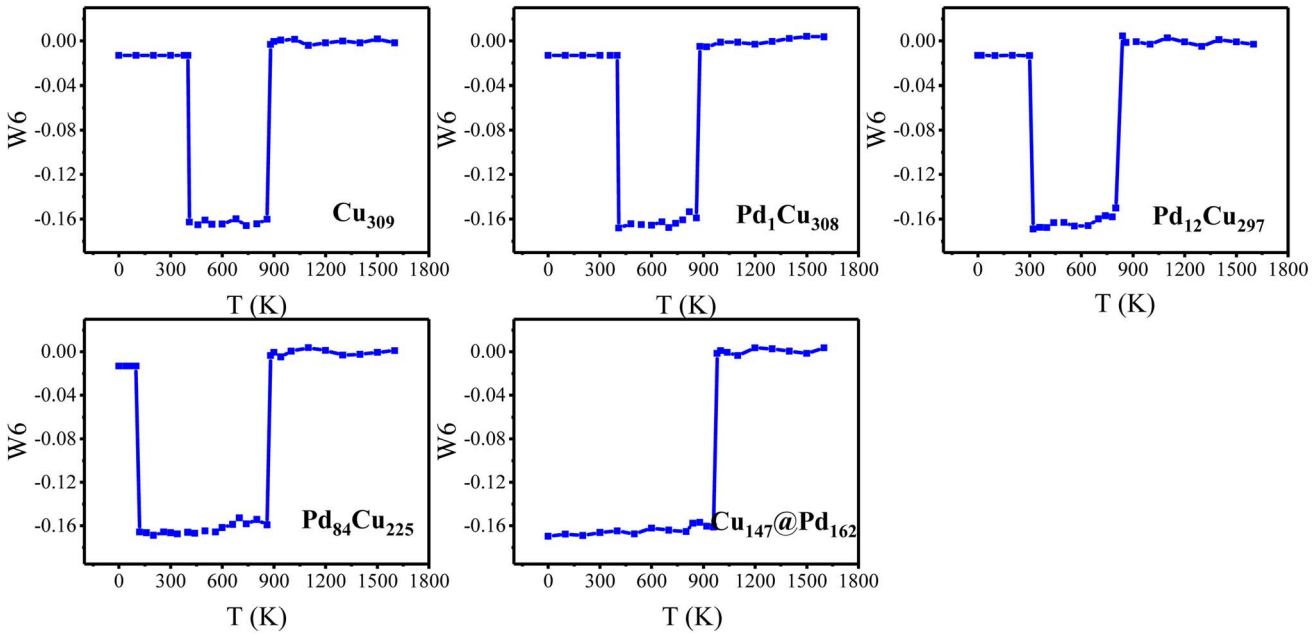

Fig. 6 The bond order *W*6 parameters *versus* the temperatures of 309-atom pure Cu, CJ-PdCu, and Cu@Pd core–shell nanoclusters with five compositions.

correlation between T_{tran} and T_{melt} and Pd-decorated concentrations at different cluster sizes in Fig. 7(a) and (b). We see a clear trend that T_{tran} decreases with the increasing Pd concentration, as shown in Fig. 7(a), which can be attributed to surface reconstruction induced by Pd doping. When Pd atoms are doped on the surface of Cu clusters, there is a large interfacial lattice mismatch between Pd and Cu atoms in alloy nanoclusters due to the different atomic radii. The dislocation thus would occur spontaneously as long as temperature-aided kinetic energy overcomes the energy barrier between structural transformations. More specifically, when Pd atoms on the cluster surface increase, there will be a larger interfacial lattice mismatch in PdCu clusters, providing the necessary driving force for Cubo–Ico structural transformation, so the Cubo–Ico transformation temperature further gets lower. When Pd composition maximizes and covers all over the NCs surface (*i.e.*, Cu@Pd), there will be a very large interfacial mismatch stress at the core–shell interface lattice site. Thus, the atomic layer adjacent to the interface slides more easily, and the ordering of lattice strain can be propagated more easily in a long-range mode, as discussed in the previous theoretical studies in the literature.[38] Hence, the Cu@Pd core–shell NCs have the lowest Cubo–Ico transition temperature.

Conversely, Pd composition seems to have a positive effect on the melting point. As shown in Fig. 7(b), the increase in T_{melt} is not straightforward from pure Cu, CJ-1, CJ-2 to CJ-3 NCs but a noticeable rise at Cu@Pd. It is associated with the higher T_{melt} of 1828 K for bulk Pd than that of 1358 K for bulk Cu, as the fraction of Pd of Cu@Pd rises evidently, and thus we see the obvious jump from CJ-3 to Cu@Pd nanocluster.

Since the surface and interface effects of nanoclusters have a significant influence on the structural evolution of clusters, we can further quantitatively characterize it by the excess energy ΔE_c,[31,39] which will be adopted to analyze the Cubo–Ico structural transition behavior. The excess energy of clusters is given by,

$$\Delta E_c = E_c - E_c^{Id} \quad (1)$$

where E_c is the average energy per atom in the nanocluster and E_c^{Id} is the average energy per atom in an infinite ideal solution with the same concentration, which is defined as:

$$E_c^{Id} = \frac{1}{N_A + N_B}[N_A E_C(A) + N_B E_C(B)] \quad (2)$$

where E_C(A) and E_C(B) are the energy per atom of A and B bulk materials at a given temperature, respectively. The bulk system is obtained by using a cubic periodic supercell with an FCC structure including 500 atoms. N_A and N_B are the total number of A and B atoms, respectively.

Taking PdCu alloy clusters with 309 atoms as an example, we show the excess energy of PdCu clusters with five compositions at different temperatures in Fig. 7(c). Some conclusions are as follows. First, we can see that the excess energy at 0 K is almost the same as that at 200 K for Cu_{309}, Pd_1Cu_{308} (CJ-1 structure), and $Pd_{12}Cu_{297}$ (CJ-2 structure) nanoclusters. As discussed above, these three nanoclusters do not undergo the Cubo–Ico transition at 0 K and 200 K, which suggests that the excess energy is independent of the temperature when the cluster does not experience the Cubo–Ico transition. Second, the excess energy of CJ-3 structured PdCu nanocluster at 200 K is lower than that at 0 K since this cluster undergoes Cubo–Ico transformation at 120 K (between 0 K and 200 K), suggesting that the release of the excess energy of PdCu clusters will lead to the Cubo–Ico structural transformation. Third, we see that the

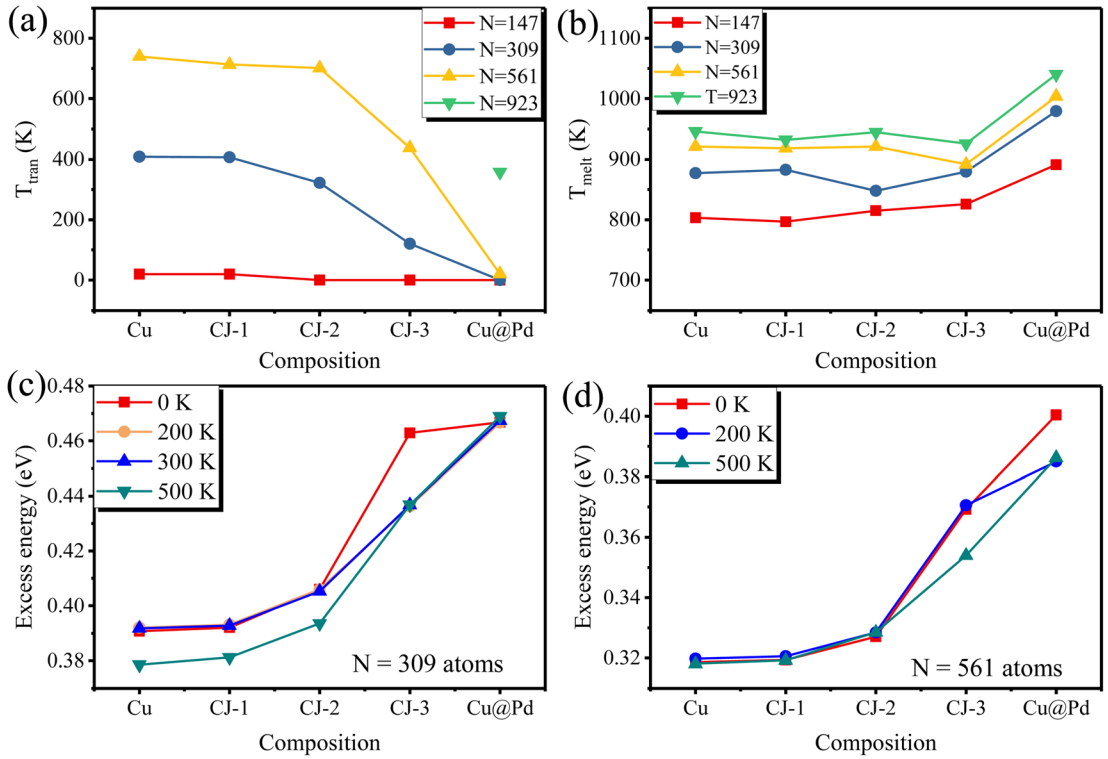

Fig. 7 (a) The Cubo–Ico structural transformation temperature (T_{tran}), (b) solid–liquid transition temperature (T_{melt}) and (c and d) excess energy *versus* Pd composition-varied Cu-based nanoclusters. Four samples with sizes ranging from 147 to 923 atoms are presented for T_{tran} in (a) and T_{melt} in (b). 309-atom (c) and 561-atom (d) samples are selected for excess energy.

excess energy at 200 K is almost identical to that at 300 K for PdCu nanoclusters with five compositions, and the cluster does not undergo the Cubo–Ico structural transition at these temperatures. Fourth, as Cu_{309}, CJ-1, and CJ-2 structures have undergone the Cubo–Ico structural transformation at 409 K, 407 K, and 322 K, respectively (between 300 K and 500 K), their excess energy at 500 K is lower than that at 300 K. This further confirms that the release of excess energy will lead to the Cubo–Ico transformation. Fifth, we found that the excess energy of $Cu_{147}@Pd_{162}$ core–shell cluster at 0 K, 200 K, 300 K, and 500 K is almost the same, which is because this cluster undergoes the Cubo–Ico structural transition at the stage of relaxation at 0 K.

Besides, we also calculated the excess energy of PdCu clusters with $N = 561$ atoms, as shown in Fig. 7(d). A similar conclusion can be reached: the excess energy of CJ-3 at 500 K is lower than that at 200 K since the cluster undergoes the Cubo–Ico transformation at 438 K (between 200 K and 500 K). The excess energy at 200 K and 500 K for the Cu@Pd cluster is lower than that at 0 K since the T_{tran} is 20 K. In a word, the Cubo–Ico structural transition is strongly related to the release of excess energy.

3.3 Size-dependent structural and solid–liquid transformation temperatures of PdCu nanoclusters

Fig. 8 exhibits the Cubo–Ico structural transition temperatures (T_{tran}) and the melting temperatures (T_{melt}) *versus* $N^{-1/3}$ (N is the number of total atoms of nanoclusters) of PdCu nanoclusters at each composition (pure Cu, three CJ structures, and Cu@Pd core–shell nanoclusters). From Fig. 8(a), we see that as the cluster size increases, T_{tran} becomes higher, indicating that the structural transformation becomes more difficult. When the cluster size increases to 923 atoms ($N^{-1/3} = 0.10277$), this Cubo–Ico structural transformation will no longer occur in some PdCu nanoclusters, which can be explained by the surface effect. With the increase of the nanocluster size, the surface effect will become weaker, and the lower surface-to-volume ratios will result in lower values of intrinsic compressive stress imposed on the nanocluster surface, thus reducing the driving force provided for the Cubo–Ico transition. Therefore, the Cubo–Ico structural transition temperature of PdCu nanoclusters rises with the increasing cluster size.

In addition, we can see from Fig. 8(b) that the melting temperature rises with the increase of PdCu cluster size for each composition. The melting point has a nearly linear relationship with $N^{-1/3}$ for all five compositions, which is in qualitative agreement with Pawlow's law.[40] Therefore, the cluster size has a significant effect on the structural transformation behavior.

As far as we know, there are no DFT or experimental reports in the literature on the particular Cubo–Ico transition in PdCu nanoalloys. However, similar Cubo–Ico structural transformations have been found in other alloy nanoclusters by MD simulations, for example, AuAg nanoclusters,[25,38] RhCu,[41] and Cu-based nanoclusters.[31] Because of the small size, it is difficult to observe the microstructural evolution of nanoclusters and

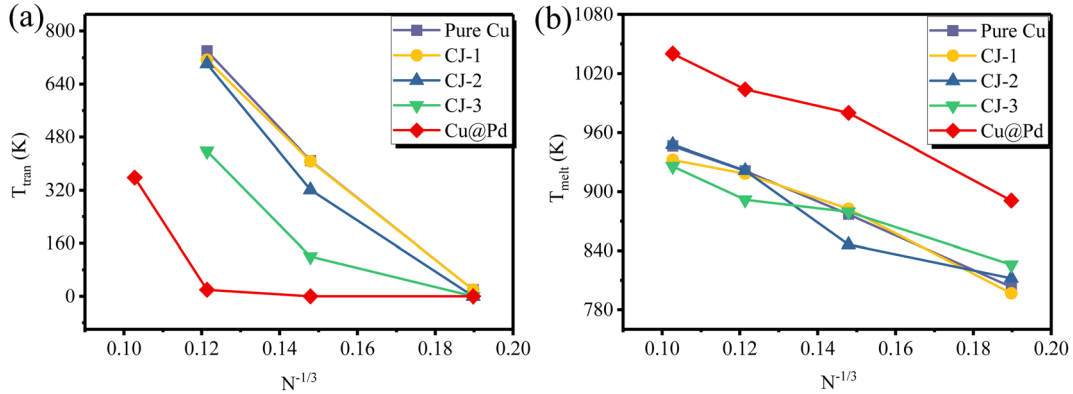

Fig. 8 (a) The Cubo–Ico structural transformation temperature (T_{tran}) and (b) the melting point (T_{melt}) as a function of the inverse cube root of size $N^{-1/3}$ for pure Cu, Pd-decorated CJ, and Cu@Pd core–shell nanoclusters.

produce well-controlled nanostructures at the atomic scale in the experiment, while MD simulation is an effective tool to achieve this. Although experimental confirmation is still scarce, our calculation provides significant guidance for the experimental study and practical application of PdCu nanoclusters.

4. Conclusions

In this study, we investigate the heating process of PdCu nanoclusters with CJ structures using MD simulations based on the EAM method and explore the influence of surface composition and cluster size on thermal stabilities and structural evolutions. Five compositions, including pure Cu cluster, three types of crown-jewel structures and core–shell structures, and four cluster sizes with N = 147, 309, 561, and 923 atoms, are used for this study. The structural transformation temperatures of these PdCu nanoclusters have been identified through the PESs, *W*6 bond order parameter, and RDFs analyses. Some PdCu nanoclusters are observed to experience the structural transition from the cuboctahedral to the icosahedral configuration before melting. We found that Cubo–Ico transition temperature decreases monotonically with the increase in Pd content of the PdCu cluster, and Cu@Pd core–shell structure always has the lowest Ico transformation temperature for each cluster size. This indicates that doping Pd atoms is beneficial to the occurrence of Cubo–Ico structural transition. Besides, with the increase in PdCu cluster size, it will become more and more difficult to experience the Cubo–Ico transformation. Finally, we also found that the cluster size has a significant impact on the melting point of PdCu clusters.

Conflicts of interest

There are no conflicts to declare.

Acknowledgements

This work was financially supported by the National Key Research and Development Program of China (Grant No. 2021YFB3802100).

References

1 Q. Liu, X. Wang, L. Li, *et al.*, Design of platinum single-atom doped metal nanoclusters as efficient oxygen reduction electrocatalysts by coupling electronic descriptor, *Nano Res.*, 2022, **15**(8), 7016–7025.
2 T. Sengupta, D. Bista and S. N. Khanna, Developing Efficient Suzuki Cross-Coupling Catalysts by Doping Palladium Clusters with Silver, *ACS Catal.*, 2021, **11**(18), 11459–11468.
3 O. Rocha-Rocha, M. Cortez-Valadez, G. Calderón-Ayala, *et al.*, Confined clustering of AuCu nanoparticles under ambient conditions, *Phys. Lett. A*, 2019, **383**(34), 125985.
4 W. Tang, L. Zhang and G. Henkelman, Catalytic activity of Pd/Cu random alloy nanoparticles for oxygen reduction, *J. Phys. Chem. Lett.*, 2011, **2**(11), 1328–1331.
5 J. Qiu, Q. N. Nguyen, Z. Lyu, *et al.*, Bimetallic Janus Nanocrystals: Syntheses and Applications, *Adv. Mater.*, 2022, **34**(1), 2102591.
6 C. Ji, Z. Luo, X. Yan, *et al.*, Enhanced-photocurrent in monolayer phototransistor with Au-SiO2 core-shell nanoparticles, *Phys. Lett. A*, 2021, **385**, 126984.
7 P. Bhatia, S. S. Verma and M. M. Sinha, Tuning the optical properties of Fe-Au core-shell nanoparticles with spherical and spheroidal nanostructures, *Phys. Lett. A*, 2019, **383**(21), 2542–2550.
8 D. Cheng, W. Wang and S. Huang, The onion-ring structure for Pd−Pt bimetallic clusters, *J. Phys. Chem. B*, 2006, **110**(33), 16193–16196.
9 H. Zhang, T. Watanabe, M. Okumura, *et al.*, Catalytically highly active top gold atom on palladium nanocluster, *Nat. Mater.*, 2011, **11**(1), 49–52.
10 X.-F. Yang, A. Wang, B. Qiao, *et al.*, Single-Atom Catalysts: A New Frontier in Heterogeneous Catalysis, *Acc. Chem. Res.*, 2013, **46**(8), 1740–1748.
11 S. Yang, J. Kim, Y. J. Tak, *et al.*, Single-Atom Catalyst of Platinum Supported on Titanium Nitride for Selective Electrochemical Reactions, *Angew. Chem., Int. Ed. Engl.*, 2016, **55**(6), 2058–2062.

12 H. Zhang, L. Lu, K. Kawashima, *et al.*, Synthesis and catalytic activity of crown jewel-structured (IrPd)/Au trimetallic nanoclusters, *Adv. Mater.*, 2015, **27**(8), 1383–1388.
13 L. Li, Y.-Z. Wang, X.-X. Wang, *et al.*, Size and Stoichiometry Effect of FePt Bimetal Nanoparticle Catalyst for CO Oxidation: A DFT Study, *J. Phys. Chem. C*, 2020, **124**(16), 8706–8715.
14 H. Zhang, L. Wang, L. Lu, *et al.*, Preparation and Catalytic Activity for Aerobic Glucose Oxidation of Crown Jewel Structured Pt/Au Bimetallic Nanoclusters, *Sci. Rep.*, 2016, **6**, 30752.
15 K. R. Reddy, K. P. Lee, A. I. Gopalan, *et al.*, Synthesis of metal (Fe or Pd)/alloy (Fe–Pd)-nanoparticles-embedded multiwall carbon nanotube/sulfonated polyaniline composites by γ irradiation, *J. Polym. Sci., Part A: Polym. Chem.*, 2006, **44**(10), 3355–3364.
16 S. Shen, T. Zhao, J. Xu, *et al.*, Synthesis of PdNi catalysts for the oxidation of ethanol in alkaline direct ethanol fuel cells, *J. Power Sources*, 2010, **195**(4), 1001–1006.
17 G. Hu, F. Nitze, E. Gracia-Espino, *et al.*, Small palladium islands embedded in palladium–tungsten bimetallic nanoparticles form catalytic hotspots for oxygen reduction, *Nat. Commun.*, 2014, **5**(1), 5253.
18 J. Chen, G. Xia, P. Jiang, *et al.*, Active and durable hydrogen evolution reaction catalyst derived from Pd-doped metal–organic frameworks, *ACS Appl. Mater. Interfaces*, 2016, **8**(21), 13378–13383.
19 M. Shao, P. Liu, J. Zhang, *et al.*, Origin of Enhanced Activity in Palladium Alloy Electrocatalysts for Oxygen Reduction Reaction, *J. Phys. Chem. B*, 2007, **111**(24), 6772–6775.
20 N. N. Kariuki, X. Wang, J. R. Mawdsley, *et al.*, Colloidal Synthesis and Characterization of Carbon-Supported Pd−Cu Nanoparticle Oxygen Reduction Electrocatalysts, *Chem. Mater.*, 2010, **22**(14), 4144–4152.
21 L. Zhang, F. Hou and Y. Tan, Shape-tailoring of CuPd nanocrystals for enhancement of electro-catalytic activity in oxygen reduction reaction, *Chem. Commun.*, 2012, **48**(57), 7152–7154.
22 E. Chiani, S. N. Azizi and S. Ghasemi, PdCu bimetallic nanoparticles decorated on ordered mesoporous silica (SBA-15)/MWCNTs as superior electrocatalyst for hydrogen evolution reaction, *Int. J. Hydrogen Energy*, 2021, **46**(50), 25468–25485.
23 M. M. Flores Espinosa, T. Cheng, M. Xu, *et al.*, Compressed intermetallic PdCu for enhanced electrocatalysis, *ACS Energy Lett.*, 2020, **5**(12), 3672–3680.
24 Q. Liu, X. Wang, L. Li, *et al.*, Catalytic activity, thermal stability and structural evolution of PdCu single-atom alloy catalysts: the effects of size and morphology, *RSC Adv.*, 2022, **12**(1), 62–71.
25 A. L. Gould, A. J. Logsdail and C. R. A. Catlow, Influence of composition and chemical arrangement on the kinetic stability of 147-atom Au–Ag bimetallic nanoclusters, *J. Phys. Chem. C*, 2015, **119**(41), 23685–23697.
26 B. C. Curley, R. L. Johnston, N. P. Young, *et al.*, Combining theory and experiment to characterize the atomic structures of surface-deposited Au309 clusters, *J. Phys. Chem. C*, 2007, **111**(48), 17846–17851.
27 J. Uppenbrink and D. J. Wales, Structure and energetics of model metal clusters, *J. Chem. Phys.*, 1992, **96**(11), 8520–8534.
28 M. S. Daw and M. I. Baskes, Embedded-atom method: Derivation and application to impurities, surfaces, and other defects in metals, *Phys. Rev. B: Condens. Matter Mater. Phys.*, 1984, **29**(12), 6443.
29 S. Plimpton, Fast Parallel Algorithms for Short-Range Molecular Dynamics, *J. Comput. Phys.*, 1995, **117**(1), 1–19.
30 X. W. Zhou, H. N. G. Wadley, R. A. Johnson, *et al.*, Atomic scale structure of sputtered metal multilayers, *Acta Mater.*, 2001, **49**(19), 4005–4015.
31 G. Li, Q. Wang, K. Wang, *et al.*, Composition, concentration and configuration dependence of the icosahedral transformations in Cu-based bimetallic clusters, *Modell. Simul. Mater. Sci. Eng.*, 2009, **17**(5), 055005.
32 Q. Li, M. Wang, Y. Liang, *et al.*, Molecular dynamics simulations of aggregation of copper nanoparticles with different heating rates, *Phys. E*, 2017, **90**, 137–142.
33 D. Schebarchov, S. Hendy and W. Polak, Molecular dynamics study of the melting of a supported 887-atom Pd decahedron, *J. Phys.: Condens. Matter*, 2009, **21**(14), 144204.
34 G. Mason, Radial distribution functions from small packings of spheres, *Nature*, 1968, **217**(5130), 733–735.
35 A. Soper, The radial distribution functions of water and ice from 220 to 673 K and at pressures up to 400 MPa, *Chem. Phys.*, 2000, **258**(2–3), 121–137.
36 R. Subbaraman and S. K. Sankaranarayanan, Effect of Ag addition on the thermal characteristics and structural evolution of Ag-Cu-Ni ternary alloy nanoclusters: Atomistic simulation study, *Phys. Rev. B: Condens. Matter Mater. Phys.*, 2011, **84**(7), 075434.
37 P. J. Steinhardt, D. R. Nelson and M. Ronchetti, Bond-orientational order in liquids and glasses, *Phys. Rev. B: Condens. Matter Mater. Phys.*, 1983, **28**(2), 784.
38 F. Chen and R. L. Johnston, Martensitic transformations in Ag–Au bimetallic core-shell nanoalloys, *Appl. Phys. Lett.*, 2008, **92**(2), 023112.
39 T. Van Hoof and M. Hou, Structural and thermodynamic properties of Ag-Co nanoclusters, *Phys. Rev. B: Condens. Matter Mater. Phys.*, 2005, **72**(11), 115434.
40 P. Pawlow, Über die Abhängigkeit des Schmelzpunktes von der Oberflächenenergie eines festen Körpers, *Z. Phys. Chem.*, 1909, **65**(1), 1–35.
41 H. Akbarzadeh, M. Abbaspour and E. Mehrjouei, Competition between stability of icosahedral and cuboctahedral morphologies in bimetallic nanoalloys, *Phys. Chem. Chem. Phys.*, 2017, **19**(22), 14659–14670.